CONTACT RESISTANCE MEASUREMENTS FOR THE $Ge_2Sb_2Te_5$ THIN FILMS

A. YAKUBOV[*], A. SHERCHENKOV, P. LAZARENKO, A. BABICH,
D. TEREKHOV, A. DEDKOVA
National Research University of Electronic Technology, Bld. 1, Shokin Square, Zelenograd, Moscow, 124498, Russia

In this study contact resistances between the $Ge_2Sb_2Te_5$ thin films and TiN/W electrodes were investigated by the transmission line model method. The influence of the heat treatment on the electrical characteristics of the $Ge_2Sb_2Te_5$/electrode was investigated. Heat treatment at 150 °C leads to a significant drop in contact resistance due to crystallization of the thin $Ge_2Sb_2Te_5$ film. The contribution of the contact resistance to the total contact resistance of the $Ge_2Sb_2Te_5$ and TiN/W contact was analyzed and showed that the contribution of the contact resistance to the total resistance sufficiently increases for the $Ge_2Sb_2Te_5$ film in the crystalline state.

1. Introduction

Phase change memory (PCM) attracts increased interest as promising new class of non-volatile memory device due to the high operation speed, low power consumption, high endurance, extended scalability, compatibility with CMOS technology [1-3].

Currently, chalcogenide semiconductor compound $Ge_2Sb_2Te_5$ (GST225) is widely used as PCM material due to high stability at room temperatures and fast crystallization rate [3-5].

The SET and RESET operations in electrical PCM is based on the reversible phase transition between the crystalline state with low resistivity and amorphous state with high resistivity. Such transitions are induced by the temperature increase caused by the electrical pulses and Joule heating.

So, in the case of PCM the total cell resistance determines the work of the memory device. The contact resistance between the phase change memory material and electrode may be responsible for the significant part of this total resistance [6] and so can seriously affect the memory performance and influence number of important parameters of PCM, such as programming characteristics [8], device switching behavior, power consumption, reliability [7-10]. The contact resistance between PCM material and metal electrodes can be responsible for the reduction of RESET current [11]. The multiple thermal cycling used for the SET/RESET operations can lead to the interaction between the phase change memory material and electrode, which can influence the stability of the PCM cell work.

The contribution of the contact resistance between the PCM material and electrodes to the total resistance of the memory cell increases with the development of the technological node and scaling down the PCM cell size [12, 13], and can seriously affect the memory performance. At last, contact resistance can be a dominating factor for the reliable work of the multi-level PCM cell.

So, for the successful implementation of the PCM technology, it is important to investigate and optimize the contact properties between the PCM material and electrodes. However, despite the intensive investigations and noticeable progress achieved last years in the development of the phase change memory technology contact properties and contact resistance of the PCM materials

---

*Corresponding author: alexsey007@mail.ru

with different electrode materials are not fully studied and obtained results have a certain discrepancy.

For the amorphous, crystalline and nanowire GST225 chalcogenide contact resistances were estimated for such conducting materials as TiW [14-17], TiN [13], refractory metal nitride electrode [18], Ti/Pt [19], Ni/Au [11]. It was demonstrated that the contact resistivity depended on the annealing temperature, applied voltage and the thickness of the PCM material film.

In this regard, the aim of the present work was the investigation of the contact resistance between the GST225 thin film and TiN/W electrode, and the influence of the heat treatment on it.

2. Experimental

Thin GST225 films were deposited on the oxidized Si substrates by dc magnetron sputtering of the stoichiometric polycrystalline target. The residual pressure in the chamber before the deposition was $3.0 \cdot 10^{-3}$ Pa, and the pressure of Ar during the process was $5.7 \cdot 10^{-1}$ Pa. The dc power was 25 W, the film thicknesses determined by the atomic force microscope (NT-MDT Solver Pro) were 130 nm.

Elemental composition of the films was determined by Auger spectroscopy (Perkin Elmer PHI-660), and results are shown in Fig. 1. Composition of the films was close to $Ge_2Sb_2Te_5$, and as can be seen from the figure, the elemental distribution was uniform across the film thickness.
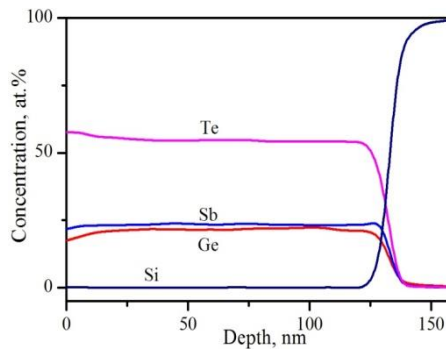
Fig. 1. Elemental distributions for the deposited film determined by Auger spectroscopy.

The structure of the GST225 films was studied by X-ray diffraction (Rigaku Smart Lab, step $\Delta\theta = 0.001$ °, scanning speed 1 ° per minute, λ (CuKα1) = 1.5406 Å). It was determined that the as-deposited and annealed at 100 °C films were in an amorphous state (Fig. 2). Thin films annealed at 200 and 250 °C for 30 min had a crystalline structure identified as NaCl with space group Fm-3m.
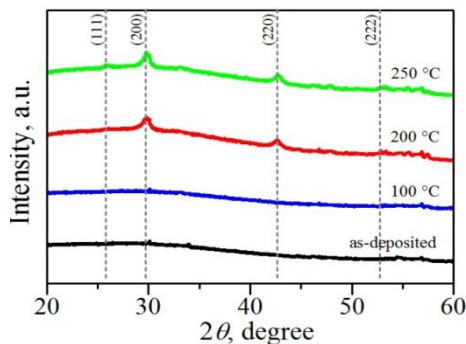
Fig. 2. Diffraction patterns of the as-deposited GST film and film after the heat treatment.

Thermal properties were investigated by differential scanning calorimetry (DSC-50, Shimadzu). For this purpose, GST225 films were deposited on c-Si substrates. Thin films were scraped from the wafers with a sapphire spatula and pressed in Al pans. Empty Al pans were used as references. Measurements were carried out at a heating rate of 5 °C/min in a nitrogen flow (20 ml/min) up to 250 °C.

The temperature dependences of the resistivity for GST225 thin films were investigated on a special set-up, containing heating stage HFS600E-PB4 Linkam and picoammeter Keithley 6485. The measurements were carried out at heating rate of 5 °C/min in an argon atmosphere up to 400 °C.

To study the influence of peculiarities of the interaction between the adjacent layers with the heat treatment on the electrical characteristics of the GST225/electrode structure, contact resistances were investigated by the transmission line model (TLM) method originally proposed by Shockley [20]. This method is well known as a simple and reliable technique for measuring contact resistance of the metal/semiconductor structure in the case of Ohmic behavior, and the resistivity of the semiconductor [10, 13, 21-24].

The TLM test structure is shown in Fig. 3. GST225 thin film was deposited on the oxidized Si substrate. Then 11 electrodes with the same geometry (length d=0.5 mm and width W=2 mm) and different distances between each other (L = 0.5, 1, 1.5, 2, 3, 4, 5, 10 mm) were fabricated. TiN/W (25/25nm) were examined as electrodes and were deposited as electrodes on the top of the GST225 thin film through the mask by the magnetron sputtering.
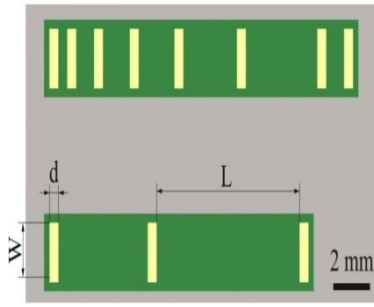
Fig. 3. TLM test structure.

According to the TLM method, the total resistance R_T between the two electrode pads used for the measurements is given by the equation [21]

$$R_T = \frac{2R_{SK}L_T}{W} + \frac{R_{SH}L}{W} \tag{1}$$

where W is the electrode width; L is the distance between two electrodes; R_{SH} and R_{SK} are the sheet resistances of the semiconductor layer outside the contact region and directly under the contact, respectively; L_t is the current transfer length defined as the length of the contact used for transferring most of the current from the semiconductor to the metal or from the metal to the semiconductor [22].

Contact resistance (R_c) of the semiconductor/electrode contact is equal to

$$R_C = \frac{R_{SK}L_T}{W} \tag{2}$$

In the case of electrically long contact d $\gg$ L_T (d is the lengths of the electrodes) and $R_{SH}=R_{SK}$ specific contact resistance (ρ_c) is determined as

$$\rho_c = R_{SH}L_T^2 \ . \tag{3}$$

By a linear fitting of the experimentally obtained dependence of total resistance (R_T) on the distance between the electrodes (d), R_c, R_{SH} and L_T can be determined from the intercept of the fitting line with the R_T and d axes and slope of the line.

TLM measurements were carried out using an Agilent E3647A power source and a Keithley 6485 picoammeter (for high-resistance amorphous samples) / Keithley 2700 multimeter (for low-resistance crystalline samples). To form an electrical contact to the samples, tungsten probes were used. Measurements were carried out between adjacent electrodes for the different electrode distances.

To study the influence of the heat treatment on the electrical characteristics of the GST225/electrode contact annealing of the TLM test structures was performed using an HFS600E-PB4 Linkam heating stage at annealing temperatures of 100, 150, 200, 250, 300 °C during 15 minutes. To prevent oxidation of the samples, annealing was carried out in an argon atmosphere.

3. Results and discussion

Fig. 4 shows resistivity temperature dependence and differential scanning calorimetry scan for GST225 thin film.
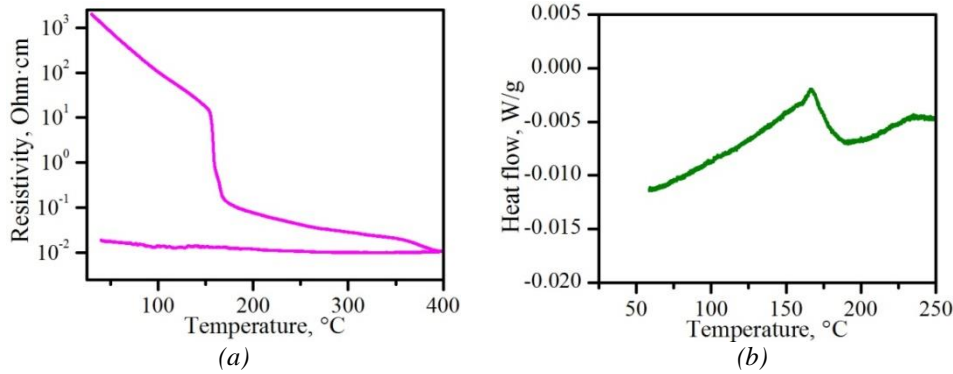
Fig. 4. Resistivity temperature dependence (a) and DSC scan (b) for the GST225 thin films.

As can be seen from the figures, in the temperature range of 152.5-172.0 °C sharp drop of the resistivity by two orders of magnitude and endothermic peak on the DSC curve are observed due to the crystallization of the amorphous film. The crystallization temperature determined from the resistivity temperature dependence by the first derivative as the highest transition rate during crystallization was estimated as 155.3 °C. The crystallization temperatures determined from the DSC curve by the tangent method was estimated as 161.2 °C.

These results correlate with the X-ray diffraction data and were used for the selection of the annealing temperatures of the TLM test structures.

Current-voltage characteristics for the TLM test structures without heat treatment are presented in Fig. 5.
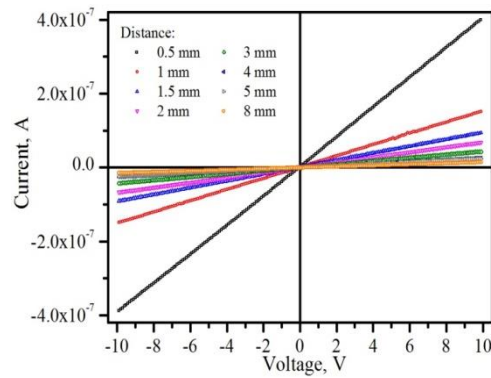
Fig. 5. I-V characteristic for the different distances between the electrodes.

As can be seen from the figure, the current-voltage characteristics are symmetric and linear ($R^2 \geq 0.99$) indicating on the Ohmic behavior and confirming the correctness of the TLM method application. It should be noted that the same Ohmic behaviors and good linear fitting were also established for all annealing temperatures used.

The total resistances R_T were obtained from the measurements of the current-voltage characteristics of the TLM test structures. Fig. 6 shows the dependences of R_T on the distance between the adjacent conducting electrodes for the different annealing temperatures, and linear fitting of these dependences.
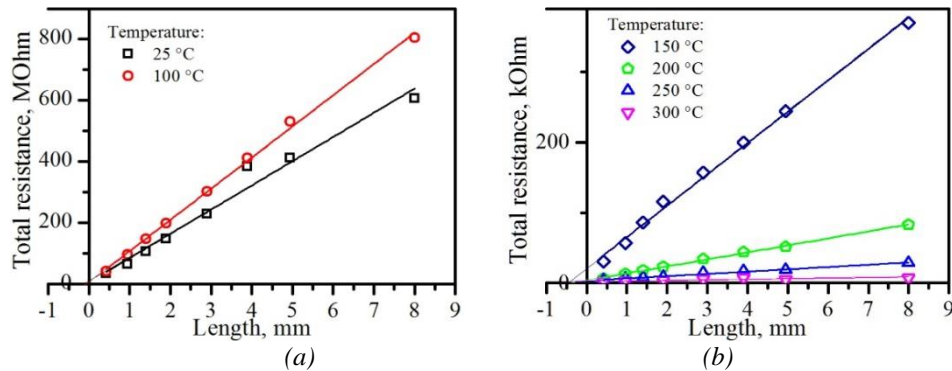
Fig. 6. Dependence of the total resistance on the distance between the electrodes:
a – amorphous state; b – crystalline state

As can be seen from the figures, these dependences are well described linearly ($R^2 \geq 0.99$). The fitting lines were used for the estimation of the transfer length L_T, contact resistance R_c and sheet resistance R_{SH} as was described in Experimental. Obtained values of L_T and R_{SH} were used for the calculation of the specific contact resistance ρ_c. Results are presented in the Table 1.

Table 1. Estimated values of R_c, L_T, and R_{SH} for annealing temperatures.

Annealing temperatures	R_c, Ohm	L_T, mm	R_{SH}, Ohm/sq	ρ_c, Ohm m^2
without	$3.30 \cdot 10^6$	0.042	$1.54 \cdot 10^8$	$2.69 \cdot 10^{-1}$
100	$2.97 \cdot 10^6$	0.029	$1.99 \cdot 10^8$	$1.69 \cdot 10^{-1}$
150	$1.02 \cdot 10^4$	0.226	$8.73 \cdot 10^4$	$4.50 \cdot 10^{-3}$
200	$1.78 \cdot 10^3$	0.179	$1.94 \cdot 10^4$	$6.22 \cdot 10^{-4}$
250	$1.64 \cdot 10^3$	0.210	$6.33 \cdot 10^3$	$2.79 \cdot 10^{-4}$
300	$1.30 \cdot 10^3$	0.410	$1.34 \cdot 10^3$	$2.25 \cdot 10^{-4}$

Fig. 7 shows the dependences of the total resistance R_T and contact resistance R_c on the annealing temperature.
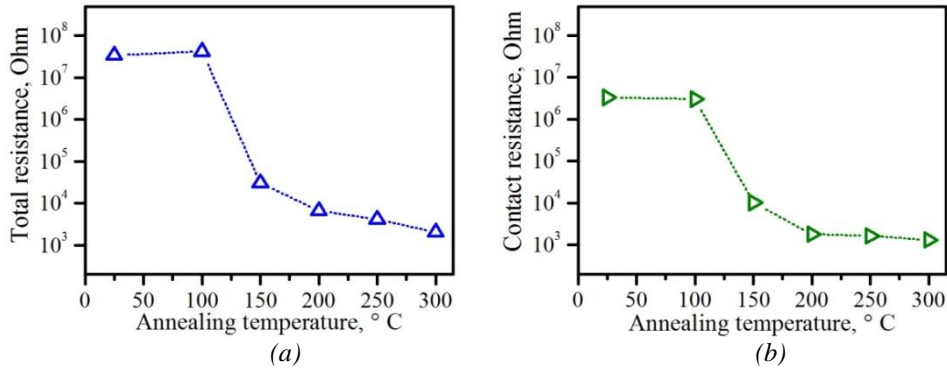
Fig. 7. Dependences of the total resistance for the GST225 films with distance between the electrodes of 0.5 mm (a) and contact resistance (b) on the annealing temperature.

As can be seen from the figure, the total resistance and contact resistance decreases by 3 and more than 2 orders of magnitude, respectively, at the annealing temperature of 150 °C. These drops correlate with the resistivity temperature dependence (Fig. 4) and are associated with a phase transition from the amorphous to the crystalline state.

Fig. 8 shows the temperature dependence of the estimated specific contact resistance.
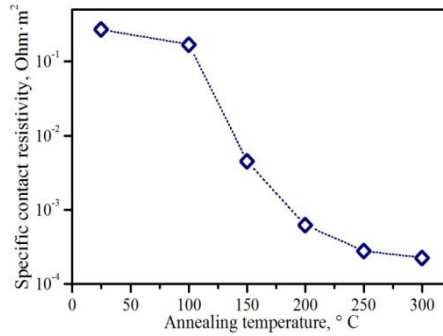
Fig. 8. Annealing temperature dependence of the specific contact resistivity for the GST225 film with TiN/W electrode.

As can be seen from the figure, heat treatment at 150 °C is accompanied by the drop of the specific contact resistivity, which is continued by the slight decrease at higher temperatures. Test structures demonstrate a change in ρ_c for the as-deposited films and annealed at 300 °C from $2.69 \cdot 10^{-1}$ to $2.25 \cdot 10^{-4}$ Ohm·m^2.

The same drop of the specific contact resistivity due to the crystallization of the PCM material was observed for $Ge_2Sb_2Te_5/TiW$ [15], Sb_2Te/W [15], nanowire $Ge_2Sb_2Te_5/TiN$ [13], $Ge_2Sb_2Te_5/W$ [25], $GeCu_2Te_3/W$ [25] contacts.

Then contribution of the contact resistance to the total resistance of the GST225/electrode structure was calculated as proportion R_c/R_T using obtained values. Fig. 9 present dependence of the proportion R_c/R_T on the annealing temperature. The total resistance was used for the distance between the TiN/W electrodes of 0.5 mm.
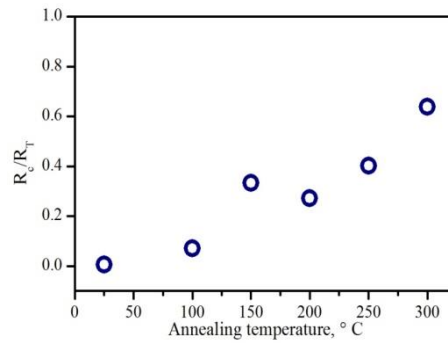
Fig. 9. Dependence of the proportion R_c/R_T on the annealing temperature.

As can be seen from the figure, the ratio R_c/R_T increases with the annealing temperature and became sufficient after the phase transition. This means that in the crystalline state, contact resistance plays a significant role in the resistance of the PCM memory cell. This result correlated with the literature data. It was shown that the contribution of the contact resistance to the total resistance is dominating for the contact of crystallized $Ge_2Sb_2Te_5$ with Pt and Pt/Ti electrodes [19], nanowire $Ge_2Sb_2Te_5$ with Ni/Au electrodes [11]. As was shown in the work [13] for the contact of nanowire $Ge_2Sb_2Te_5$ with TiN the contact resistance dominates in the total resistance for the small film thicknesses that are smaller than 1μm in both crystalline and amorphous states.

4. Conclusions

Thus, in this study, contact resistances between the GST225 thin film and TiN/W electrode was investigated by the transmission line model method.

The influence of the heat treatment on the electrical characteristics of the GST225/electrode was investigated. Heat treatment at 150 °C leads to the drop of the specific contact resistivity from $2.69 \cdot 10^{-1}$ to $4.50 \cdot 10^{-3}$ Ohm·m^2. Further heat treatment up to the temperature of 300 ° C leads to the further drop of ρ_c $2.25 \cdot 10^{-4}$ Ohm·m^2.

The contribution of contact resistance to the total resistance of the $Ge_2Sb_2Te_5$ and TiN/W electrode contact was analyzed, and showed that the contribution of the contact resistance dominates for the Ge2Sb2Te5 film in the crystalline state.

Acknowledgements

References

[1] J. H. Kim, D. S. Byeon ,D. H. Ko , J. H. Park, Thin Solid Films **659**, 1 (2018).

[2] A. Sherchenkov, S. Kozyukhin, A. Babich, P. Lazarenko, Journal of Non-Crystalline Solids **377**, 26 (2013).

[3] G. W. Burr, M. J. Breitwisch, M. Franceschini, D. Garetto, K. Gopalakrishnan, B. Jackson, B. Kurdi, C. Lam, L. A. Lastras, A. Padilla, B. Rajendran S. Raoux, R. S. Shenoy, J. Vac. Sci. Technol. B. **28**(2), 223, (2010).

[4] S. Raoux, W. Wełnic, D.Ielmini, Chem. Rev. **10**(1), 240 (2010).

[5] N. Yamada, E. Ohno, N. Akahira, K. Nishiuchi, K. Nagata , M. J. Takao, J. Appl. Phys. **26**(S4), 61 (1987).

[6] F. Xiong, E. Yalon, A. Behnam, C.M. Neumann, K.L. Grosse, S. Deshmukh, E. Pop, in IEDM Tech. Dig. **1**, 1 (2016).

[7] D. L. Kenche, I. V. Karpov, B. G. Johnson, S. J. Lee, D. Kau, S. J.Hudgens, J. P. Reifenberg, S. D. Savransky, J. Zhang, M. D. Giles, G. Spadini, in IEDM Tech. Dig. **1**, 323 (2007).

[8] A. L. Lacaita, Solid-State Electronics. **50**(1), 24 (2006).

[9] C. Cabral, K. N. Chen, L. Krusin-Elbaum, V. Deline, Appl. Phys. Lett. **90**(5), 051908 (2007)

[10] D. H. Kang, I. H. Kim, J. H. Jeong, B. K. Cheong, J. Appl. Phys. **100**(5), 054506 (2006).

[11] I. Hwang, Y. J. Cho, M .J. Lee, M. H. Jo, Appl. Phys. Lett. **106**(19), 193106 (2015).

[12] C. W. Jeong, D. H. Kang, D. W. Ha, Y. J. Song, J. H. Oh, J. H. Kong, J. H. Yoo, J. H. Park, K. C. Ryoo, D. W. Lim, S. S. Park, J. I. Kim, Y. T. Oh, J. S. Kim, J. M. Shin, J. Park, Y. Fai, G. H. Koh, G. T. Jeong, H. S. Jeong, K. Kim, Solid State Electronics, **52**(4), 591 (2008).

[13] R. Huang, K. Sun, K. S. Kiang, R. Chen, Y. Wang, B. Gholipour, D. W. Hewak, C. H. De Groot, Semicond. Sci. Technol. **29**(9), 095003 (2014).

[14] D. Roy, M. A. A. in't Zandt, R. A. M. Wolters, C. E. Timmering, J. H. Klootwijk, In2009 10th Annual Non-Volatile Memory Technology Symposium (NVMTS). IEEE, 12 (2009).

[15] D. Roy, M. A. A. in't Zandt, R. A. M. Wolters, IEEE Electron Device Lett. **31**(11), 1293   10).

[16] D. Roy, J. H. Klootwijk, D. J. Gravesteijn, R. A. M. Wolters, Proceedings of the Solid-State Device Research Conference (ESSDERC), 87 (2011).

[17] E. K. Chua, R. Zhao, L. P. Shi, T. C. Chong, T. E. Schlesinger, J. A. Bain, Appl. Phys. Lett. **101**(1), 012107 (2012).

[18] S. D. Savransky, I. V. Karpov, MRS Online Proceedings Library Archive, **1072** (2008).

[19] S. Deshmukh, E. Yalon, F. Lian, K. E. Schauble, F. Xiong, I. V. Karpov, E. Pop, IEEE Transactions on Electron Devices, **66**(9), 3816 (2019).

[20] W. Shockley, A. Goetzberger, R. M. Scarlett, Report No. A1-TOR-64-207, Air Force Atomic Laboratory, Wright-Patterson Air Force Base, Ohio, (1964).

[21] G. K. Reeves, H. B. Harrison, IEEE Electron Device Lett. **3**(5), 111 (1982).

[22] T. Abbas, L. Slewa, Int. J. Nanoelectronics and Materials **8**, 111 (2015).

[23] D. K. Schroder, Semiconductor Material and Device Characterization, 3rd ed. John Wiley & Sons, Hoboken, Arizona State University, New Jersey (2006).

[24] M. Devika, N. K. Reddy, F. Patolsky, K. R. Gunasekhar, J. of Appl. Phys. **104**(12), 124503 (2008).

[25] S. Shindo, Y. Sutou, J. Koike, Y. Saito, Y. H. Song, Materials Science in Semiconductor Processing **47**, 1 (2016).